Effect of two ion species on the propagation of shear Alfvén waves of small transverse scale

S. T. Vincena, G. J. Morales, and J. E. Maggs
Department of Physics and Astronomy, University of California, Los Angeles,
Los Angeles, California 90095, USA

The results of a theoretical modeling study and experimental investigation of the propagation properties of shear Alfvén waves of small transverse scale in a plasma with two ion species are reported. In the two ion plasma, depending on the mass of the heavier species, ion kinetic effects can become prominent, and significant parallel electric fields result in electron acceleration. The theory predicts the appearance of frequency propagation gaps at the ion-ion hybrid frequency and between harmonics of the lower cyclotron frequency. Within these frequency bands spatial structures arise that mix the cone-propagation characteristics of Alfvén waves with radially expanding ion Bernstein modes. The experiments, performed at the Basic Plasma Science Facility (BaPSF) at UCLA, consist of the spatial mapping of shear waves launched by a loop antenna. Although a variety of two ion-species combinations were explored, only results from a helium-neon mix are reported. A clear signature of a shear wave propagation gap, as well as propagation between multiple harmonics, is found for this gas combination. The evanescence of shear waves beyond the reflection point at the ion-ion hybrid frequency in the presence of an axial magnetic field gradient is also documented. © *2010 American Institute of Physics*. [doi:10.1063/1.3422549]

I. INTRODUCTION

In a cold magnetized plasma two different electromagnetic waves can propagate[1,2] for a specified frequency. In general, one wave propagates with a faster speed than the other, thus a reasonable nomenclature for them would be "fast mode" and "slow mode." Unfortunately, depending on the specific frequency band, different research communities use a different terminology to distinguish between these two modes. This practice can be confusing when comparing results across different research areas, especially when more complicating features are considered, such as finite ion and electron temperatures and multiple ion species. In a sense, the present study falls in this category. Thus, it is useful to define, at the outset, the wave modes that are being investigated. For a single ion species, and in the frequency band near the ion cyclotron frequency, the two, cold-plasma electromagnetic modes are most commonly known as "Alfvén waves." In the laboratory-oriented community, the slower mode is frequently described as the "shear" Alfvén wave, and the faster mode as the "compressional" Alfvén wave. The present study focuses entirely on the shear mode.

This investigation examines the propagation properties of shear Alfvén waves of small transverse scale in plasmas consisting of two ion species. Here, by small scale it is meant that the characteristic dimension of the wave fields across the confinement magnetic field is small compared to the ion-skin depth c/ω_{pi}, where c is the speed of light and ω_{pi} is the largest ion plasma frequency. The interest in the small transverse scales is that they can result in large electric fields, both parallel and perpendicular to the confinement magnetic field. Waves in this regime give rise to plasma heating and/or particle acceleration. For this reason, these modes are of interest to fusion,[3,4] space,[5,6] and solar researchers.[7,8] A simplifying feature of this regime of small transverse scale is

that the compressional mode is evanescent for those frequencies for which the shear wave propagates.

The propagation properties of shear Alfvén modes of small transverse scale have now been extensively investigated in laboratory plasmas with a single ion species and for uniform confinement magnetic fields.[9–13] Modes excited by a small source propagate along the magnetic field in a spreading headlight pattern[14–16] bounded by cones whose small angle relative to the confinement magnetic field depends on the wave frequency. As the frequency approaches the ion cyclotron frequency, the cone angle widens and the mode does not propagate far from the source due to its low parallel velocity and concomitant damping by electrons and ions. Similar features have also been observed in toroidal magnetic fields.[17]

When two ion species are present, the transverse component of the cold plasma dielectric, $\varepsilon_\perp$, can vanish at a frequency whose value lies between the cyclotron frequencies of the two species, where $\varepsilon_\perp$ is infinite. The frequency for which $\varepsilon_\perp = 0$ depends on the relative concentration of the ion species and it is widely known as the ion-ion hybrid frequency,[18,19]

$$\omega_{ii} = \sqrt{\frac{\omega_{p1}^2 \Omega_2^2 + \omega_{p2}^2 \Omega_1^2}{\omega_{p1}^2 + \omega_{p2}^2}}, \tag{1}$$

where Ω_s and ω_{ps} are the ion cyclotron and ion plasma frequencies of species s.

Considerable attention has been devoted to the collective resonance associated with ω_{ii} in the context of wave propagation across the magnetic field.[20–23] It is expected that when the wave frequency ω matches the condition $\omega = \omega_{ii}$ somewhere in a plasma, large electric fields arise that produce major effects. Since this resonance refers to perpendicular (i.e., cross-field) propagation, it is readily accessible to the

compressional mode that propagates isotropically, but not to the shear mode that propagates mainly along the magnetic field.

The effect of the ion-ion hybrid frequency on the propagation of shear waves can be appreciated by examining the reduced (but quite accurate) dispersion relation for the parallel wave number

$$k_{\parallel} = k_0 \sqrt{\varepsilon_{\perp}} [1 - k_{\perp}^2/k_0^2 \varepsilon_{\parallel}]^{1/2}, \tag{2}$$

where $k_0 = \omega/c$, $\varepsilon_{\parallel}$ is the parallel dielectric coefficient, and $k_{\perp}$ is the transverse wave number, set by a small source. Equation (2) indicates that for this mode the condition $\omega = \omega_{ii}$ (i.e., $\varepsilon_{\perp} = 0$) results in a cutoff rather than a resonance. The consequence is that for a cold plasma with two ion species, the shear mode propagates in two frequency bands separated by a gap. That is, it propagates for frequencies below the heavy ion gyrofrequency, $\omega < \Omega_1$, and for frequencies above the ion-ion hybrid frequency but below the ion gyrofrequency of the lighter ion, $\omega_{ii} < \omega < \Omega_2$. When the mode propagates in the second band, i.e., $\omega > \omega_{ii}$, it is given various names in literature, e.g., proton whistler,[24] ion cyclotron wave (ICW),[25] electromagnetic ICW,[26] and Alfvén ion-ion hybrid mode.[27] In this study we refer to it simply as the shear Alfvén mode.

The cutoff and associated propagation gap can have important consequences in various areas of plasma science. Recent studies in a tokamak[25] have identified that the compressional Alfvén wave can excite, via mode conversion,[28] a shear wave that propagates away from the ion-ion hybrid cutoff toward the low-field side of the device. This in turn has consequences for current drive, plasma heating, and flow-drive[29] scenarios in fusion devices. In the auroral ionosphere the S3-3 satellite detected[26] shear Alfvén waves excited by the auroral electron beam, but only at altitudes above the ion-ion hybrid cutoff for a hydrogen-helium plasma. A theoretical study[30] has argued for the existence of wave resonators in general planetary magnetospheres due to wave reflections at the ion-ion hybrid cutoffs straddling the planetary equator. Evidence for the ion-ion hybrid cutoff has been provided by experiments in toroidal devices[31,27] and consequences extracted for the coupling of antennas at the plasma edge.

When finite ion temperatures are included, as may be appropriate for the small transverse scales of interest, the condition $\varepsilon_{\perp} = 0$ can be satisfied for other frequency values besides ω_{ii}. These frequencies correspond to those of pure, electrostatic ion Bernstein modes[32] and have values between harmonics of the heavy ion cyclotron frequency, Ω_1. Thus, in this regime the cold propagation gap is modified by the appearance of multiple propagation bands, the number being determined by the ratio Ω_2/Ω_1. The theoretical studies reported in this manuscript illustrate the effect of these features on the propagation of shear Alfvén waves excited by a small source. It is to be noted that the results reported here pertain to fully electromagnetic signals. They are to be contrasted with previous studies of pure electrostatic modes[33–35] under plasma conditions that do not support the propagation of Alfvén waves.

The experiments reported in this study are performed in the upgraded large plasma device (LAPD-U) at the Basic Plasma Science Facility (BaPSF) at the University of California, Los Angeles (UCLA). They consist of the spatial mapping of shear waves launched by a loop antenna. A variety of two ion-species combinations were explored by mixing the basic gases helium, neon, argon, and hydrogen. All of these mixtures were found to generate highly reproducible plasmas in which propagation bands below the ion cyclotron frequency of each of the two species could be identified. However, in this paper, only results from a helium-neon mix are reported. A clear signature of a shear wave propagation gap, as well as propagation between multiple harmonics, is found for this gas combination. The evanescence of shear waves beyond the reflection point at the ion-ion hybrid frequency in the presence of an axial magnetic field gradient is also documented.

The manuscript is organized as follows. Section II presents a theoretical description of shear wave propagation in two ion-species plasmas of relevance to the experimental observations. The experimental setup is explained in Sec. III. Experimental measurements are shown in Sec. IV. A discussion of the results is found in Sec. V.

II. THEORY

To examine the properties of shear Alfvén waves in the presence of two ion species it is envisioned that an idealized source at frequency ω generates a parallel current, of small amplitude, with a prescribed spectrum of wave numbers $k_{\perp}$ transverse to the uniform confinement magnetic field $B_0\hat{z}$. The idealized source is assumed to be azimuthally symmetric and located at the origin of a cylindrical coordinate system with unit vectors $(\hat{r}, \hat{z}, \hat{\theta})$. It is of interest to calculate the spatial pattern of the signals as they propagate away from the source, i.e., the dependence on (r, z). In this geometry, and for the shear polarization, a quantity that summarizes the wave features is the azimuthal component of the perturbed magnetic field,

$$B_{\theta}(r,z,t) = \tfrac{1}{2}\tilde{B}_{\theta}(r,z)e^{-i\omega t} + \text{c.c.} \tag{3}$$

In this analysis, the simplest model source[14] is considered. It consists of a cylindrical disk of radial dimension, a, to which an oscillatory potential is applied to draw a plasma current, I, oscillating at frequency ω. In spite of its simplicity, the model has been found to provide an accurate description of experimental observations[9] and computer simulation results.[16] More elaborate sources (e.g., not azimuthally symmetric) can be modeled by the linear superposition of the patterns radiated by several replicas of this basic source. It is noteworthy that more involved analysis[36] of extended loop antennas essentially display the features delineated by the simple disk model.

The radiated azimuthal magnetic field is given by[14]

$$\tilde{B}_{\theta} = \frac{2\tilde{I}}{ca} \int_0^{\infty} dk \frac{\sin(ka)}{k} J_1(kr) e^{ik_{\parallel}(k)z}. \tag{4}$$

In Eq. (4), a Bessel–Fourier representation is used with the dummy variable, k, representing the transverse wave number,

and J_1 is the Bessel function of order 1. The wave properties are contained in the parallel wave number $k_\parallel = k_\parallel(\omega, k)$, to be determined from a suitable dispersion relation.

The dispersion relation in Eq. (2) provides an excellent description for the shear wave except in a small frequency interval close to the ion cyclotron frequency[14] and can be used to extract all the essential features of wave behavior, even for plasmas with two ion species. However since the possibility of ion species having arbitrary mass ratios and finite temperature is considered, the response close to several cyclotron harmonics may be sampled. Thus, it is judicious in this application to use the full dispersion relation that retains the cross-field current due to the relative slippage between the electron $E \times B$ drift and the magnetized ion orbits. Of course, the effect of this slippage becomes more important as the ion temperature T_i increases.

From the general expression for electromagnetic wave propagation in a uniform magnetized plasma,

$$\vec{k} \times \vec{k} \times \vec{E} = -k_0^2 \overleftrightarrow{\varepsilon} \cdot \vec{E}, \tag{5}$$

where $\overleftrightarrow{\varepsilon}$ is the magnetized plasma dielectric tensor, a quadratic relationship can be obtained for the indices of refraction $n_\perp = k_\perp / k_0$ and $n_\parallel = k_\parallel / k_0$, namely,

$$0 = -n_\perp^2 n_\parallel^2 (n^2 - \varepsilon_\perp) + (n_\perp^2 - \varepsilon_\parallel)$$
$$\times [(n_\parallel^2 - \varepsilon_\perp)(n^2 - \varepsilon_\perp) - \varepsilon_{xy}\varepsilon_{yx}], \tag{6}$$

where $n^2 = n_\parallel^2 + n_\perp^2$. Defining a useful combination of auxiliary variables, this quartic equation can be shown to yield the closed-form solution,

$$n_\parallel^2 = \varepsilon_\perp + \frac{(\pm)[b^2 + 4\alpha d]^{1/2} - b}{2\alpha}, \tag{7}$$

with

$$\alpha = \varepsilon_\parallel / \varepsilon', \quad b = n_\perp^2 [(\varepsilon_\parallel + \varepsilon_\perp)/\varepsilon'],$$
$$d = \varepsilon_{xy}\varepsilon_{yx} - n_\perp^2 \varepsilon_\perp / \varepsilon', \tag{8}$$

and where $\varepsilon' \equiv \varepsilon_\parallel - n_\perp^2$. The choices $\pm$ select the two types of modes, i.e., shear and compressional.

The desired expression for the parallel wave number can be obtained from $k_\parallel = n_\parallel \omega / c$ after Eq. (7) is evaluated for the relevant plasma conditions. Since in this study the ratio of kinetic to magnetic energy density, β, satisfies the condition $\beta \gtrsim 2m/M_s$, where m is the electron mass and M_s refers to the mass of either ion species, s; the parallel electron response must be described kinetically. Accordingly, the parallel dielectric coefficient is represented as

$$\varepsilon_\parallel = 1 - \frac{k_D^2}{2k_\parallel^2} Z'\left(\frac{\omega}{\sqrt{2}k_\parallel \bar{v}_e}\right), \tag{9}$$

where k_D is the Debye wave number, $\bar{v}_e$ is the electron thermal velocity, and Z' corresponds to the derivative of the plasma dispersion function.

For the small transverse scales of interest, the perpendicular dielectric coefficients must include the transverse kinetic response of the ions. This can be important for the contribution due to the heavier ion species because the wave

frequency can be comparable to a harmonic of its cyclotron frequency. The kinetic effects due to parallel ion motion are not significant because for the experimental conditions investigated, $\omega \gg k_\parallel \bar{v}_s$, where $\bar{v}_s$ is the ion thermal velocity of species s. Thus, the relevant expressions are

$$\varepsilon_\perp = 1 + \left(\frac{\omega_{pe}}{\Omega_e}\right)^2 - 2\sum_s \left(\frac{\omega_{ps}}{k_\perp \rho_s}\right)^2 \sum_{l=1}^\infty \frac{e^{-(k_\perp \rho_s)^2} I_l(k_\perp^2 \rho_s^2)}{\omega^2 - (l\Omega_s)^2} \tag{10}$$

and

$$\varepsilon_{xy} = -i\left[\frac{\omega_{pe}^2}{\omega\Omega_e} + \sum_s \frac{\omega_{ps}^2 \Omega_s}{\omega} \sum_{l=1}^\infty \frac{e^{-(k_\perp \rho_s)^2}(I_{l+1} + I_{l-1} - 2I_l)l^2}{\omega^2 - (l\Omega_s)^2}\right], \tag{11}$$

where ω_{pe} is the electron plasma frequency, ω_{ps} is the ion plasma frequency of the s ion species, Ω_e is the electron cyclotron frequency, and $\rho_s = \bar{v}_s / \Omega_s$. In Eq. (11) the argument of the modified Bessel function of order l, I_l, is $(k_\perp \rho_s)^2$, as in Eq. (10), but not shown. It is to be noted that the imaginary part arising at the exact harmonic resonances $\omega = l\Omega_s$ is not included because the bandwidth of such resonances is less than 0.01 of the wave frequency and thus would require a high-precision measurement to isolate them.

The numerical evaluation of the integral in Eq. (4) implements an iterative scheme to determine the required $k_\parallel(k_\perp, \omega)$. For given values of $(k_\perp, \omega)$ the first pass uses the warm-electron fluid expression for $\varepsilon_\parallel$ in Eq. (2) to obtain an analytic expression

$$(k_\parallel^2)_1 = \frac{k_0^2 \varepsilon_\perp [1 + (k_\perp c/\omega_{pe})^2]}{1 + (k_\perp/k_D)^2 \varepsilon_\perp}. \tag{12}$$

This results in $(k_\parallel)_1$ which is used to form the argument of the Z' function in Eq. (9). To expedite the procedure, this function is evaluated using the two-pole approximation.[37] This procedure generates a kinetic, parallel dielectric coefficient that includes electron Landau damping. This updated $\varepsilon_\parallel$ is then used in Eq. (7) to extract the desired $k_\parallel(k_\perp, \omega)$. If more accuracy is needed, this value of $\varepsilon_\parallel$ can be used as the starting point for a new iteration.

Next, the principal features predicted by the previously described analysis are illustrated for nominal parameters used in the experimental study reported in Sec. IV. The three panels in Fig. 1 display contours (color online) in frequency-radial position space (ω, r) of the magnitude of the fluctuating magnetic field $|\tilde{B}_\theta(r, z, \omega)|$ at a fixed axial position $z = 4$ m from a source launching a signal at frequency ω. The radial extent of the source is $a = 1$ cm. In the laboratory such a figure is generated by making a radial scan with a small magnetic loop probe to measure the amplitude of the wave magnetic field for a given frequency. The process is sequentially repeated over a desired range of frequencies that include the cyclotron frequencies of the two relevant ion species. The parameters correspond to a confinement magnetic field $B_0 = 750$ G, electron density $n_e = 10^{12}$ cm^{-3}, electron temperature $T_e = 5$ eV, and cold ions, i.e., $T_i = 0$. The figure illustrates the appearance of a
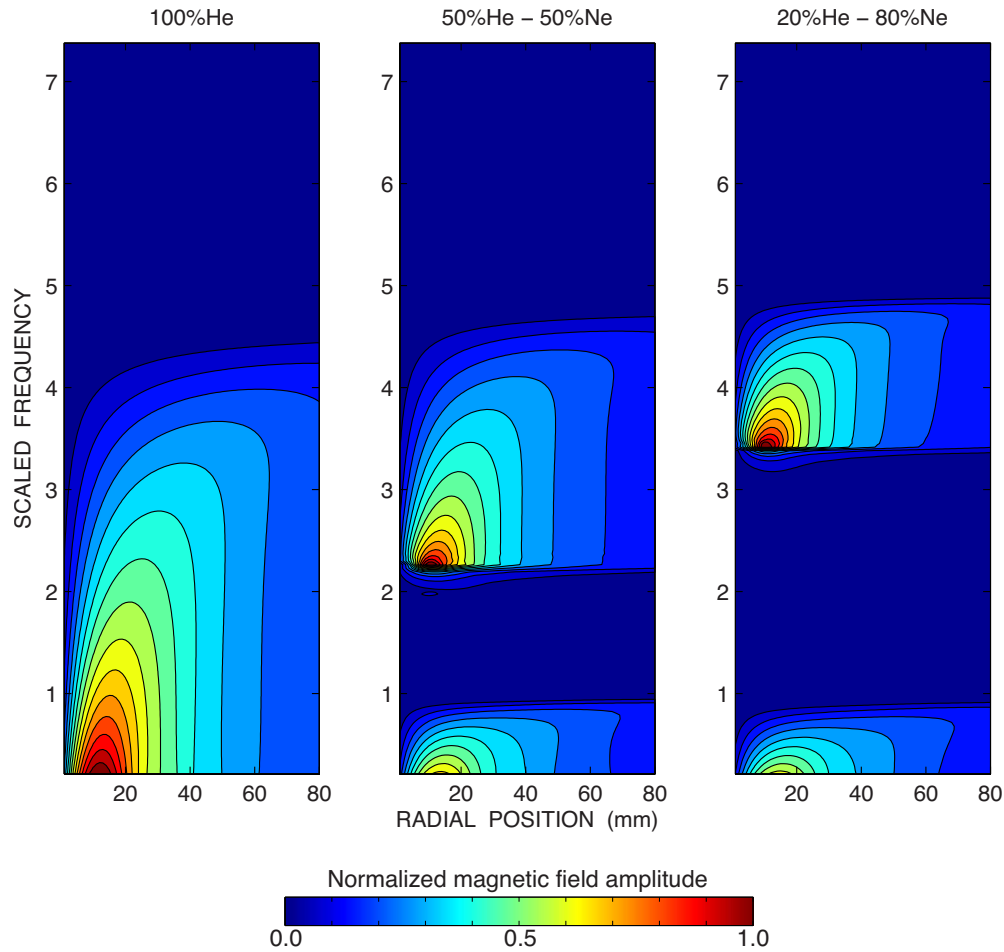
FIG. 1. (Color online) Effect of helium-neon concentration for cold-ion plasma ($T_i = 0$). Contours in frequency-radial position space (ω, r) of the magnitude of the fluctuating magnetic field $|\tilde{B}_\theta(r, z, \omega)|$ at a fixed axial position $z = 4$ m from a source launching a signal at frequency ω. Left panel is pure-helium plasma, center 50% helium-50% neon, and right 20% helium-80% neon. Frequencies are scaled to the neon cyclotron frequency.

frequency gap, determined by the ion-ion hybrid frequency, within which shear Alfvén waves do not propagate in a helium-neon species mix. The left panel corresponds to a pure-helium plasma, the center one to a 50% helium-50% neon mixture, and the right panel to 20% helium-80% neon. The electron density is fixed at $n_e = 10^{12}$ cm^{-3}. In addition to the frequency gap, the three panels illustrate the radial bending of the signals as the frequency approaches the individual cyclotron frequencies; a feature arising due to the axial group velocity becoming progressively smaller. It should be noted that the helium cyclotron frequency is five times that of neon. Also note that the small-scale radial structure in the radiation pattern ($r < 8$ cm) is small when compared to the shortest ion inertial length, which is 45 cm, corresponding to the pure-helium case.

Figure 2 illustrates the modifications produced by finite ion temperature to the characteristic cold-ion pattern shown in the center panel of Fig. 1. Figure 2 correspond to a 50% helium-50% neon plasma for the same nominal parameters. In this case the frequency range of the cold-plasma gap lies between the fundamental of the neon cyclotron frequency and the second harmonic. The left panel is for $T_i = 0$ and the right panel for $T_i = 1$ eV. It is seen that for finite ion temperature, there are signals within the ion-ion hybrid gap that

can propagate, but they exhibit a pattern different from that of the cold-ion shear Alfvén waves. In addition, new propagation bands appear between the higher harmonics of the neon cyclotron frequency. These features consist of a mixture of the properties associated with pure ion Bernstein modes[32–34] and the conelike propagation characteristics[9,14] of shear Alfvén waves of small transverse scale.

Figure 3 shows the changes produced on the frequency pattern by increasing the ion temperature. The magnitude of the wave magnetic field $|\tilde{B}_\theta(r, z, \omega)|$ is sampled at a fixed spatial position $z = 4$ m and $r = 3$ cm for a 50% helium-50% neon plasma over a frequency range spanning the cyclotron frequencies of both species. The bottom panel is the cold-ion result ($T_i = 0$), the center panel is for $T_i = 1$ eV, and the top panel for $T_i = 5$ eV. Dashed lines A–C correspond to frequencies whose spatial patterns are shown in Fig. 4. A deep frequency gap is evident for cold ions, but as the ion temperature is increased the gap fills with propagating modes. Propagation bands appear between harmonics of the neon cyclotron frequency and become progressively sharper as the ion temperature increases.

Figure 4 displays contours (color online) of the two-dimensional pattern (z, r) of the magnitude of the wave mag-
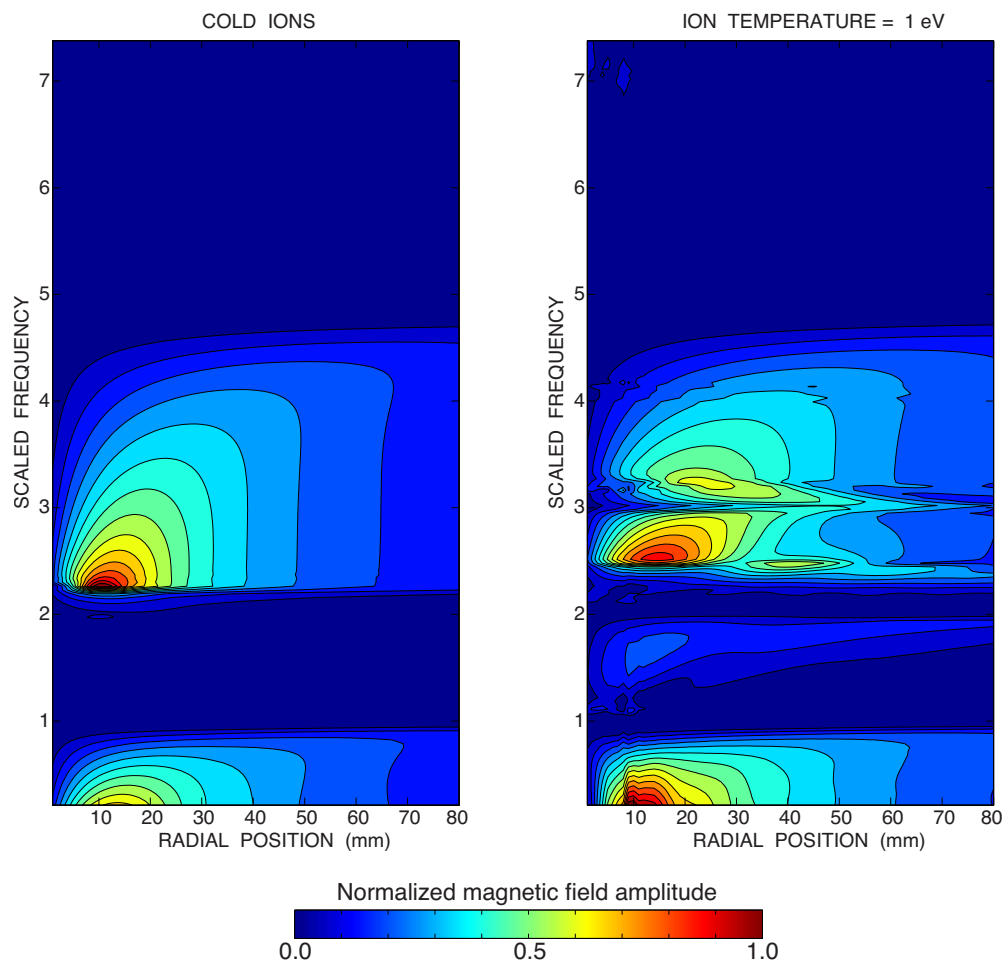
FIG. 2. (Color online) Modifications produced by finite ion temperature to the characteristic cold-ion pattern presented in Fig. 1 for a 50% helium-50% neon plasma. Left panel is for $T_i=0$ and right panel for $T_i=1$ eV. New features consist of a mixture of the properties associated with pure ion Bernstein modes and the conelike propagation characteristics of shear Alfvén waves of small transverse scale.

netic field $|\tilde{B}_\theta(r,z,\omega)|$ for selected frequencies corresponding to dashed lines A–C in Fig. 3. The values of the frequencies have been chosen to lie just below and above the cyclotron harmonics of neon to illustrate the relationship to Bernstein wave properties. The reference patterns are shown in the bottom panels; they are for the same frequency as the panel just above. The bottom panels exhibit the classic features well known for a cold ($T_i=0$), single ion-species (helium) plasma, and for the same nominal parameters used in the previous figures. The angle of propagation relative to confinement magnetic field (z-direction) is seen to increase progressively as the frequency approaches the He cyclotron frequency. However, for the 50% helium-50% neon plasma with $T_i=1$ eV (corresponding to the top panels), the patterns change radically as the frequency passes across harmonics of the neon cyclotron frequency.

To further emphasize the topological change in propagation, Fig. 5 displays the two-dimensional (z,r) phase contours (color online) associated with these waves. The bottom panels show the clear signature of predominantly field-aligned propagation commonly associated with shear Alfvén waves. In contrast, the response for frequency B, corresponding to $\omega=2.2\Omega_{Ne}$, displays phase fronts that propagate across the confinement magnetic field, as is characteristic of ion

Bernstein modes. For frequency A, at $\omega=1.8\Omega_{Ne}$, a combination of the previous two extreme cases appears. Finally, for case C, at $\omega=3.2\Omega_{Ne}$, the field-aligned propagation begins to emerge.

III. EXPERIMENTAL SETUP

A. Plasma device

These experiments are conducted in the LAPD-U (Ref. 38) at the Basic Plasma Science Facility at the University of California, Los Angeles. This is a cylindrical device with an overall length of 2070 cm and a main chamber diameter of 100 cm. A simplified schematic of the experimental arrangement is shown in Fig. 6. The plasma is produced using an electrical discharge between a heated, oxide-coated nickel cathode and a molybdenum mesh anode on one end of the device, while an electrically floating copper mesh terminates the plasma at the far end. The main plasma column between the conducting mesh boundaries is 1660 cm in length and carries no net current. The typical column diameter is 60 cm, measured at the full width at half-maximum value of a perpendicular density profile. Highly reproducible plasma dis-
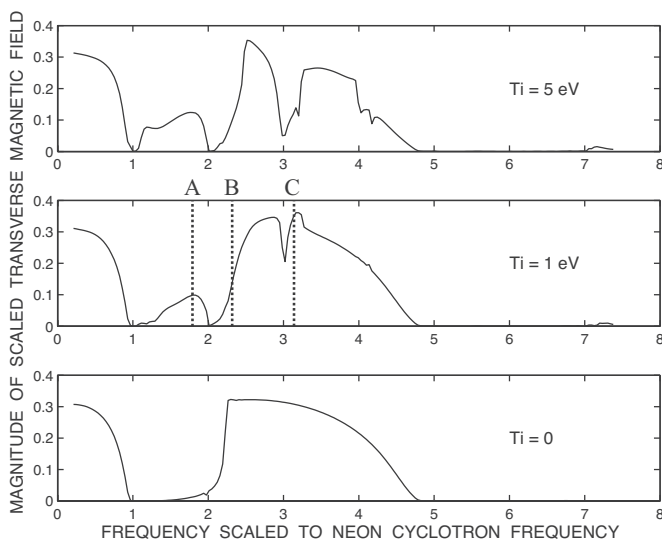
FIG. 3. Changes produced on the frequency pattern by increasing the ion temperature. Magnitude of the wave magnetic field $|\tilde{B}_\theta(r,z,\omega)|$ at a fixed spatial position $z=4$ m and $r=3$ cm for a 50% helium-50% neon plasma. Bottom panel shows cold-ion gap ($T_i=0$). Center panel is for $T_i=1$ eV and top for $T=5$ eV. Dashed lines correspond to (z,r) patterns in Figs. 4 and 5.

charges 15 ms long are repeated at 1 Hz; this allows for the collection of large ensemble data sets using probes with computer-controlled drives.

The plasma densities are typically $(1-3)\times10^{12}$ cm^{-3}, as measured using a swept Langmuir probe calibrated with a microwave interferometer. Electron temperatures are 5–8 eV during the main plasma discharge (also measured with the swept probe.) Ion temperatures are approximately 1 eV, measured variously with a gridded energy analyzer, Fabry–Pérot interferometer, and laser-induced fluorescence (in argon). The confining axial magnetic field is produced with a set of solenoidal electromagnets controlled by ten separate power supplies. The device is typically run with a uniform magnetic field strength of 300–2000 G, but the independent supplies allow for a variety of field configurations, with a peak field of 3000 G.

B. Production of two ion plasmas

Various gas mixtures are produced using fixed-flow settings in independent mass flow controllers that regulate the partial pressures of the individual gases: hydrogen, helium, neon, and argon. Four turbomolecular pumps provide a steady-state pumping speed to produce a constant neutral fill pressure to within the error of measurement of both an ion gauge and a commercial quadrupole mass spectrometer. Generally, the partial pressures of the neutral gases do not reflect the relative concentration of the ion densities so that another method must be adopted to determine the ion densities.

For plasmas with low density ($n<10^{10}$ cm^{-3}), low temperature ($T_e<4$ eV, $T_i<0.1$ eV), and with low ionization fraction ($\sim0.1\%$), the spectroscopic-Langmuir method, described by Ono et al.,[39] may be employed to measure the concentration ratio of the two ion densities. This method relies on the existence of a linear relationship between the

optical intensity of a carefully chosen *neutral* emission line and the number density of the corresponding plasma ion. Linear calibration curves are used to relate the ion saturation current measurements (hence density) in pure neon and helium plasmas to their corresponding neutral line intensities. Then, in the mixed plasmas, either the intensity ratio between the two neutral lines or the intensity of one line and the electron density are used to determine the ionization fraction of the two ions. This method depends on the existence of a linear relationship between ion saturation current and neutral line intensity. However, the relationship becomes nonlinear above 10^{10} cm^{-3} in the pure neon plasma. In the present experiment, the higher densities ($\sim10^{12}$ cm^{-3}) and higher ionization fraction (50%) make the spectroscopic-Langmuir technique unsuitable.

In many laboratory experiments with two ion species, the observed frequency of the ion-ion resonance provides the most accurate method to determine the ionization fraction of the two species. In the present experiment, the ionization fraction is heavily used as an experimental parameter so that without *a priori* knowledge of the results, a separate method is needed to determine a desired mixture. A convenient and widely used method is to assume that the ionization fraction is equal to the ratio of the neutral fill pressures. In the present experiment, however, a modification of this procedure is implemented. In the steady-state discharge, with an electron temperature of T_e, the density of a particular ion species n_i is assumed to be described by $n_i=N_i\exp(-e\Phi_i/T_e)$, where the neutral density is N_i and Φ_i is the first ionization potential for the given atom. The neutral gases are taken to be isothermal so that the ratio of the neutral densities equals the ratio of the partial pressures: $N_1/N_2=P_1/P_2$. The partial pressures P_i are measured using the mass spectrometer. The ionization fraction is then given by

$$\frac{n_1}{n_2}=\frac{P_1}{P_2}\exp(-e\Delta\Phi_{12}/T_e),\tag{13}$$

with $\Delta\Phi_{12}$ being the difference in ionization potentials. The ions are assumed to be singly ionized and that charge neutrality holds: $n_1+n_2=n_e$. The ratio of neutral densities is established by adjusting the mass flow controllers until the desired ratio is achieved. The absolute values of the partial pressures are iteratively adjusted to maintain a constant electron density of 1×10^{12} cm^{-3} as measured using a microwave interferometer.

The efficacy of this technique will be apparent in the presentation of experimental results. When compared to ion mixture ratios derived from the wave propagation characteristics, it results in mixtures close to the desired ratios with a systematic error.

C. Wave excitation and measurement

The waves are launched with a loop antenna. It consists of a bare copper rod (0.48 cm in radius) bent into three legs of a rectangle and placed in the chamber, as shown in Fig. 6. The internal, axial leg extends along $\mathbf{B}_0$ at the center of the plasma column. The perpendicular legs extend out of the
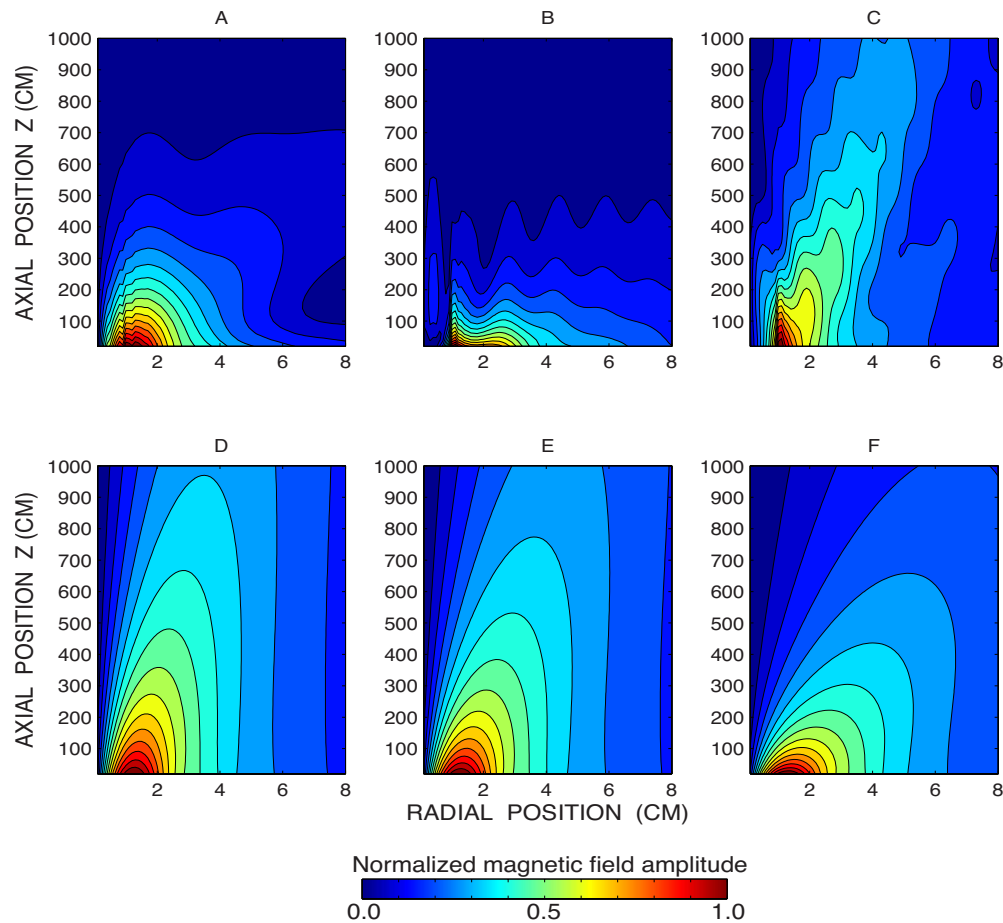
FIG. 4. (Color online) Contours of the two-dimensional pattern (z,r) of the magnitude of the wave magnetic field $|\tilde{B}_\theta(r,z,\omega)|$ for selected frequencies corresponding to the dashed lines A–C in Fig. 3. Bottom panels are for a pure-helium plasma and cold ions $(T_i=0)$. Top panels are for a 50% helium-50% neon plasma with $T_i=1$ eV. Note the difference between axial scale (10 m) and radial scale (8 cm).

chamber via vacuum feedthroughs. The current path is closed with copper wire, which also forms one side of a one-to-one isolation transformer. The second side of the transformer is connected to the output of a 2 kW rf amplifier. A programmable function generator drives the amplifier input. The generator is operated in a gated-on mode to drive a tone burst at a specified frequency during a 2 ms time window. This window begins 3 ms before the shutoff of the cathode-anode discharge. Previous studies, conducted in plasmas with a single ion species, have documented the radiation of shear Alfvén waves from this type of antenna.[40,41] The azimuthal magnetic field, produced by the magnetic field-aligned leg of the antenna current, couples to a propagating shear Alfvén wave. The currents in the radially aligned antenna legs slightly break the symmetry assumed in the theoretical description, but are not observed to couple to shear waves or other plasma modes.

Wave magnetic fields are measured using magnetic induction probes (i.e., B-dot loops). These probes are constructed of pairs of oppositely wound induction coils with 0.3 cm diameter loops of 50 turns each. A probe comprises three such coil pairs with each orthogonal pair measuring the time varying magnetic field along a Cartesian direction. The signals from each coil pair are combined using a differential amplifier of gain 10 to remove electrostatic pickup. The linearity and response of each amplified coil pair is tested using a commercial network analyzer and the known field of a Helmholtz coil. The calibration data are in the form of amplitude and phase as functions of frequency. The probe response is measured to be linear in the range of frequencies used in these experiments.

The time series data for each probe are digitized at 12.5 MHz and recorded with a 14 bit resolution. Using the phase-locked experimental setup and reproducibility of the background plasma, the time series from between two and eight plasma discharges are averaged together before storage to improve the signal-to-noise ratio. After storage, each probe can be automatically moved (using computer-controlled stepper motors) to a new spatial location, or the wave frequency can be changed as desired, and the process repeated. Since the recorded voltages are proportional to dB/dt, the signals are numerically integrated to produce $B(t)$. Integration is performed by multiplying the fast Fourier transform of each Hanning-windowed time series, together with the calibration data appropriate for each probe signal. The result is either transformed back to the time domain, or the relevant amplitude of B at the driving frequency is extracted directly.
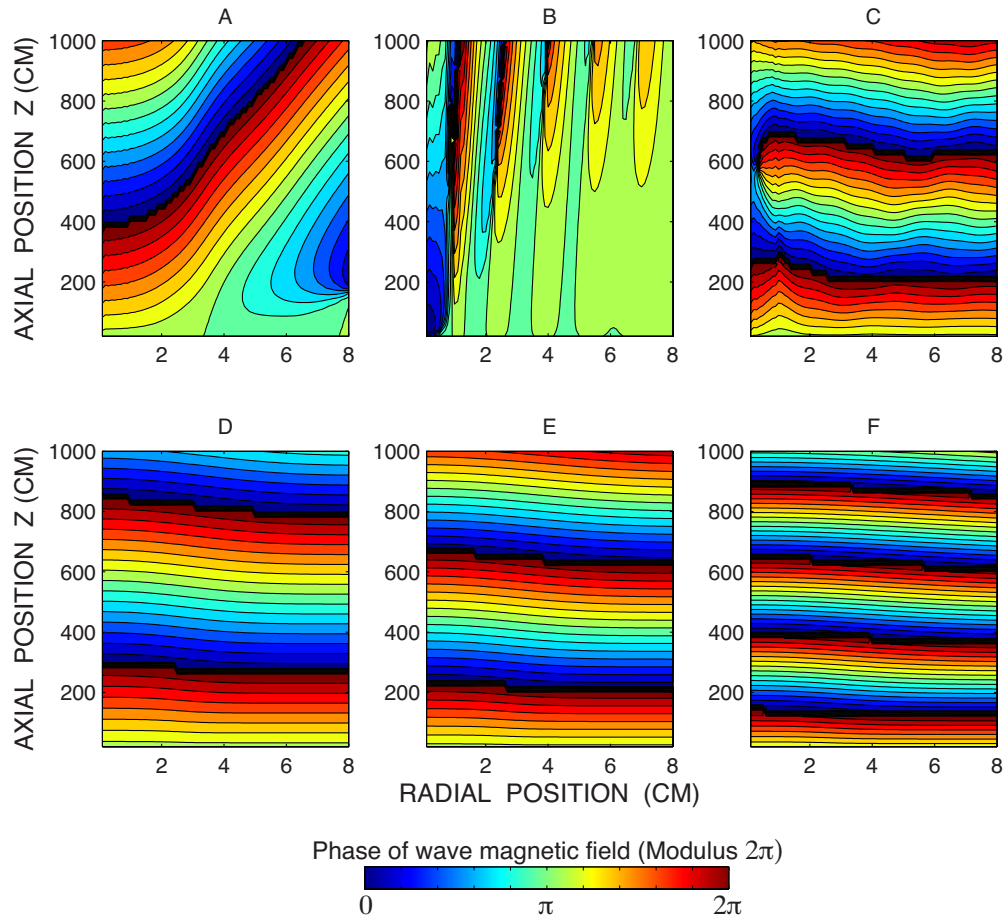
FIG. 5. (Color online) Two-dimensional (z,r) phase contours associated with the wave amplitudes shown in Fig. 4.

IV. EXPERIMENTAL RESULTS

Figure 7 shows the amplitude of the y-component of the measured magnetic field as a function of frequency and position across the plasma column for a plasma with a mixture set at a concentration of 50% helium and 50% neon, as determined by Eq. (13). Under the conditions of these experiments the y-component corresponds to the azimuthal wave field. The data are taken at an axial position 4.8 m from the source antenna with uniform axial field strength of 750 G. The top panel of Fig. 7 is a contour plot (color online) illus-

trating the existence of two propagation bands, one below the neon gyrofrequency at 57 kHz and one between the ion-ion hybrid frequency at 128 kHz and the helium gyrofrequency at 285 kHz. An ion Bernstein wave feature is also visible between the first and second harmonics of the neon gyrofrequency. The bottom panel of Fig. 7 shows the radial profile of the amplitude of the y-component of the magnetic field for three frequencies; one at 40 kHz in the lower shear wave band, one at 105 kHz near the ion Bernstein feature, and one at 190 kHz in the upper shear wave band. The radial
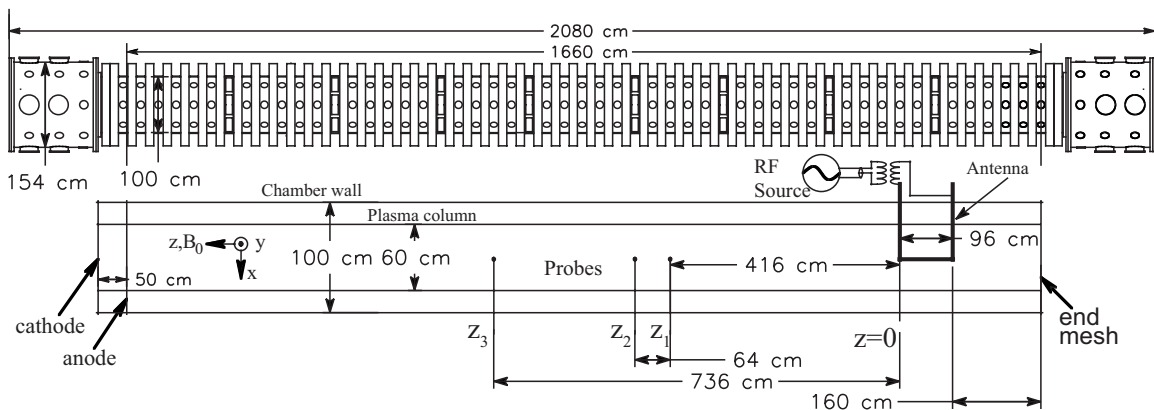

FIG. 6. Top is a side view of LAPD-U showing vacuum chamber, solenoidal magnet placement, and circular and rectangular access ports. Bottom is a schematic of the experimental arrangement showing the loop antenna and the locations of the B-dot probes used to measure the wave fields.
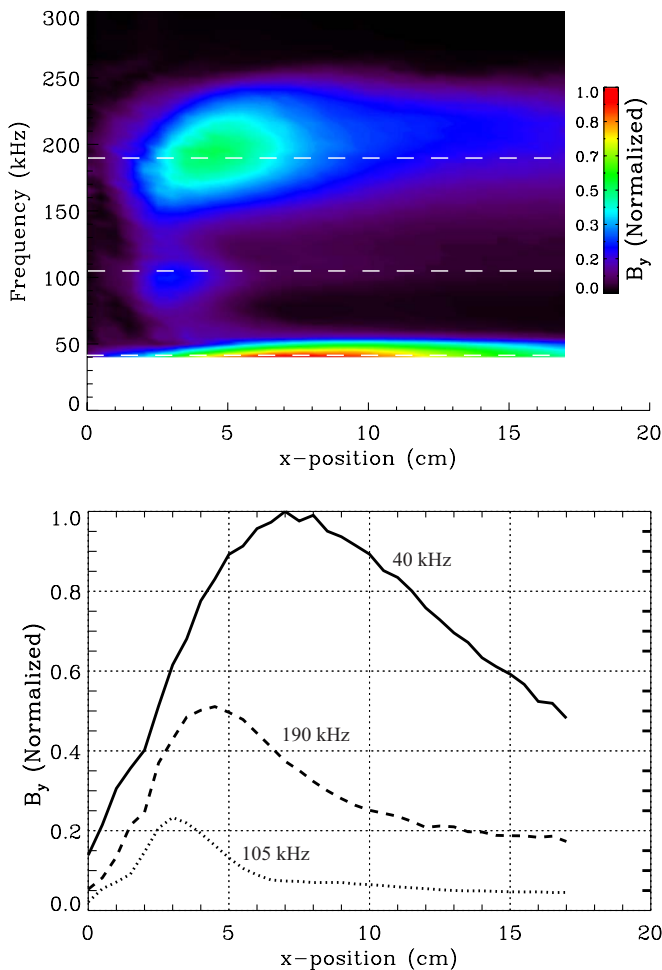
FIG. 7. (Color online) Top: contour of the amplitude of the *y*-component of the wave magnetic field as a function of frequency and position across the plasma column for a 50% helium-50% neon plasma at a location 4.8 m from the source in a 750 G axial field. Bottom: radial profiles of amplitude of the wave magnetic field for the frequencies indicated by the dashed lines in the top panel.

FIG. 8. Amplitude of the *y*-component of the wave magnetic for a 50% helium-50% neon mixture as a function of normalized frequency at an axial distance 4.8 m and radial location 1 cm from the source, showing structure between the harmonics of the Ne gyrofrequency.

frequency profile of the amplitude of the *y*-component of the magnetic field is shown at a spatial location 2 cm from the source center, and axial distance 4.8 m, for various concentration ratios. The concentration ratios range from 50% neon-50% helium to 85% neon-15% helium. From Eq. (1) the ion-ion hybrid frequency can be written as

$$f_{ii} = f_{c2}\left(\frac{M_2}{M_1}\right)^{1/2}\left(\frac{\rho_1 M_1 + \rho_2 M_2}{\rho_1 M_2 + \rho_2 M_1}\right)^{1/2}, \qquad (14)$$

where f_{c2} is the ion cyclotron frequency of ion "2" and ρ_2 is the concentration ratio of ion 2 (i.e., $\rho_2 = n_2/n$, is the ratio of the density of ion 2 to the total plasma density). From Eq. (14) it can be deduced that as the concentration of neon (ion "1") relative to helium (ion 2) increases ($\rho_1 -> 1; \rho_2 -> 0$), the upper shear wave propagation band becomes narrower ($f_{ii} -> f_{c2}$), and disappears altogether for the pure neon

profile of the Bernstein feature differs from those of the shear waves in that it peaks near the source and has an extended radial pattern. The main peak for all three patterns lies well within the plasma column radius of 30 cm, which is less than the 64 cm helium ion inertial length for this case.

The appearance of Bernstein wave features in the data is elucidated in Fig. 8. The amplitude of the *y*-component of the wave magnetic field is shown for a 50% He-50% Ne mixture as a function of frequency normalized to the neon ion gyrofrequency. Since the amplitude of the Bernstein features peak near field lines connected to the source, the data shown in Fig. 8 are taken at a spatial location 1 cm from the field line on which the source is located. The detailed shape of the frequency profile depends on radial location, and the Bernstein feature is not readily apparent at all radial locations. Bernstein modelike structures are evident in the bands between the first and second, and the fourth and fifth neon harmonics. These data are the analog of the theoretical profile shown in the center panel of Fig. 3.

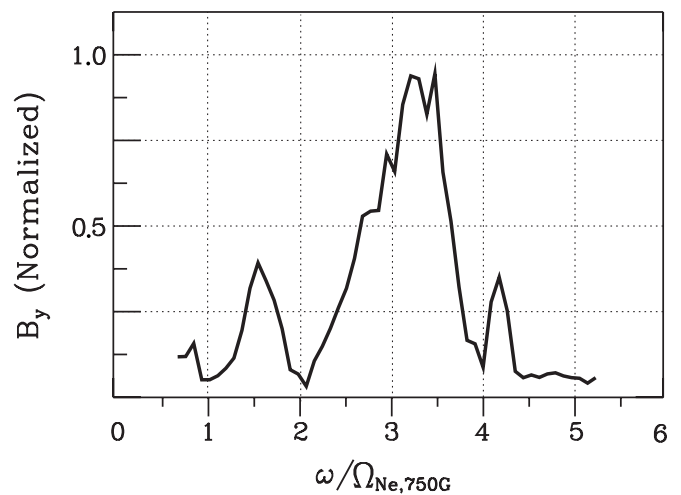Figure 9 shows the effects of changing the concentration ratio of the mixture of the two ions, helium and neon. The
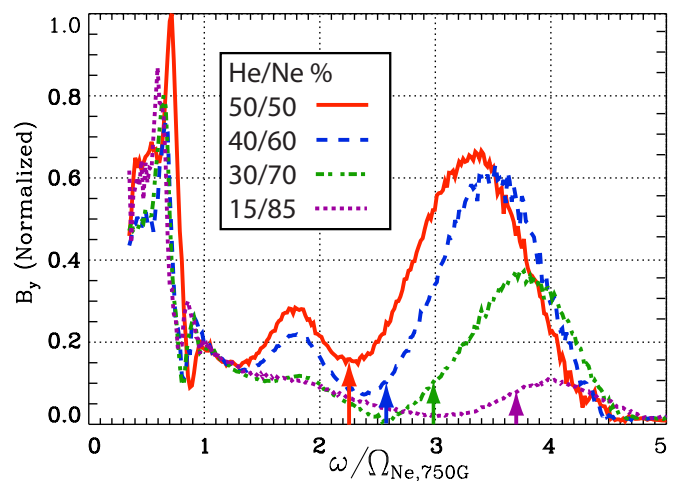

FIG. 9. (Color online) Frequency profile of the amplitude of the *y*-component of the magnetic field at a spatial location 2 cm from the source center, and axial location 4.8 m, for various concentration ratios, as indicated. The cutoff frequency predicted by Eqs. (13) and (14) is indicated by vertical arrows.

plasma. Figure 9 clearly shows the tendency for the upper propagation band to narrow with increasing neon concentration. However, the lower cutoff of the propagation band is not sharp and the amplitude of the waves in the upper band decreases significantly.

The vertical arrows along the bottom axis of Fig. 9 indicate the frequencies at which the ion-ion hybrid cutoff would occur for the given concentration ratios. The concentration ratios listed in Fig. 9 are based on the technique given in Eq. (13). On the other hand, using the properties of wave propagation, the ion-ion hybrid frequency should be identified as the lowest propagating frequency in the upper band. Thus one might identify the minimum in the wave frequency profiles, just above the Bernstein feature as the ion-ion hybrid, in which case the technique based on Eq. (13) consistently gives too high a frequency. However, it is clear that the Bernstein feature influences the shape of the amplitude profiles for the higher concentrations of helium so that the minimum amplitude of the shear wave, without the Bernstein feature, would likely occur at lower frequency. Also, these measurements are taken at an axial position 4.8 m from the source so that the evanescent waves have not fully decayed away. Therefore, for the lower helium concentration ratios where the Bernstein feature exerts less influence on the amplitude profile, the ion-ion hybrid frequency is probably higher than the frequency at which the minimum in the amplitude occurs. Taking these last two points into consideration, the technique based on Eq. (13) likely gives a fairly good value of the ion-ion hybrid frequency, but with a systematic overestimate.

Equation (14) also indicates that the ion-ion hybrid frequency is directly proportional to the axial magnetic field strength so that an increase in B_0 results in a proportional increase in f_{ii}. Therefore, a shear wave propagating in the upper band could encounter a reflection point if it propagates into a region of larger magnetic field strength. Beyond the reflection point the wave is evanescent. To test this possibility experimentally, the confinement magnetic field is configured with a steplike change in the axial direction of the device, as illustrated in Fig. 10. In the antenna region, the magnetic field strength is 750 G, and within a few meters along the plasma column it increases to a value of 1250 G. Waves launched from the antenna can propagate in the band from $f_{ii}(750 \text{ G})$ to $f_{ci}(750 \text{ G})$ while those in the high-field region can propagate over the range $f_{ii}(1250 \text{ G})$ to $f_{ci}(1250 \text{ G})$. Thus, at axial locations where the field strength is 1250 G (the high-field region), waves with frequencies in the range $f_{ii}(750 \text{ G}) < f < f_{ii}(1250 \text{ G})$ should be evanescent. The only waves propagating in the high-field region should be those in the frequency band $f_{ii}(1250 \text{ G}) < f < f_{ci}(750 \text{ G})$, where the lower frequency limit is due to the ion-ion hybrid cutoff, and the upper limit is the largest shear wave frequency that can be launched at the antenna. It is to be noted that these frequency propagation bands are determined using the local dispersion relations, derived for a uniform plasma; as such, they should be viewed as approximations unless far from the gradient region. The details of the wave propagation in the nonuniform plasma require a differential or an integral equation formulation.
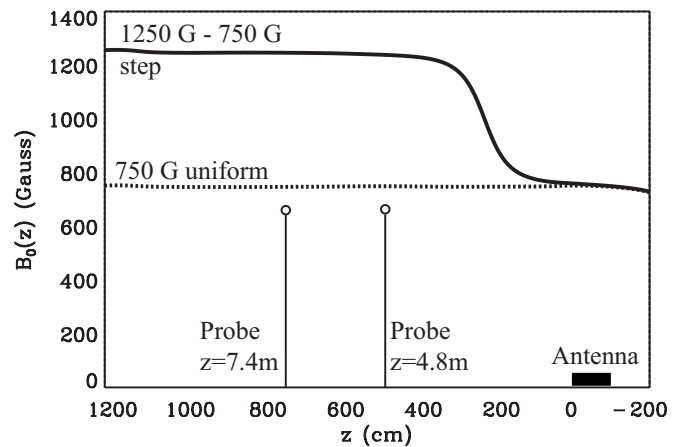

FIG. 10. Schematic of the magnetic step used in obtaining the data shown in Figs. 11 and 12. The strength of the axial magnetic field varies from 750 G at the antenna to 1250 G in the uniform region 5 m away. Waves whose frequency matches the ion-ion hybrid frequency in the connecting ramp are reflected. The positions of the B-dot probes are indicated.

The observed behavior of waves propagating into the magnetic step is presented in Figs. 11 and 12. Figure 11 compares contours of the amplitude of the y-component of the wave magnetic field as functions of launched frequency and position across the plasma column. Measurements are taken at two axial positions from the antenna, 4.8 m for the panels on the right, and 7.4 m for the left panels. Both correspond to locations within the uniform high-field side of the step. The contours shown in the top panels of Fig. 11 are for the case of a step in the magnetic field, while those in the bottom panel are for a uniform 750 G axial field, i.e., no step. Notice that the spreading of wave energy across the magnetic field is much more pronounced in the uniform field case as compared to the magnetic step. Also, the narrowing of the propagation band for the nonuniform case is evident, and is indicative of the evanescence of waves launched from the source at frequencies below $f_{ii}(1250 \text{ G})$. The structure in the amplitude centered around 175 kHz, very evident in the data in the top-left panel, is apparently a Bernstein mode feature just below the second harmonic of neon in the high-field region.

The evanescence of waves propagating into the high-field region is also illustrated on the top panel of Fig. 12, which presents the frequency profiles, at a fixed radial location 2 cm from the source, of the amplitude of the y-component of the wave magnetic field, measured in the high-field region at axial positions of 4.8 and 7.4 m from the antenna. For comparison, these same profiles, for the uniform field case, are shown at the bottom panel of Fig. 12. In both cases, the amplitude at the position farthest from the source (7.4 m) is set to match the amplitude at the position nearest the source (4.8 m) at 300 kHz (the highest frequency measured). The expected evanescence of shear waves propagating in the upper band in the frequency range $f_{ii}(750 \text{ G}) < f < f_{ii}(1250 \text{ G})$ can be discerned by noting that the amplitude of waves measured at the axial position 7.4 m from the source is well below the amplitude at the axial location 4.8 m from the source, for frequencies below $f_{ii}(1250 \text{ G})$. On the
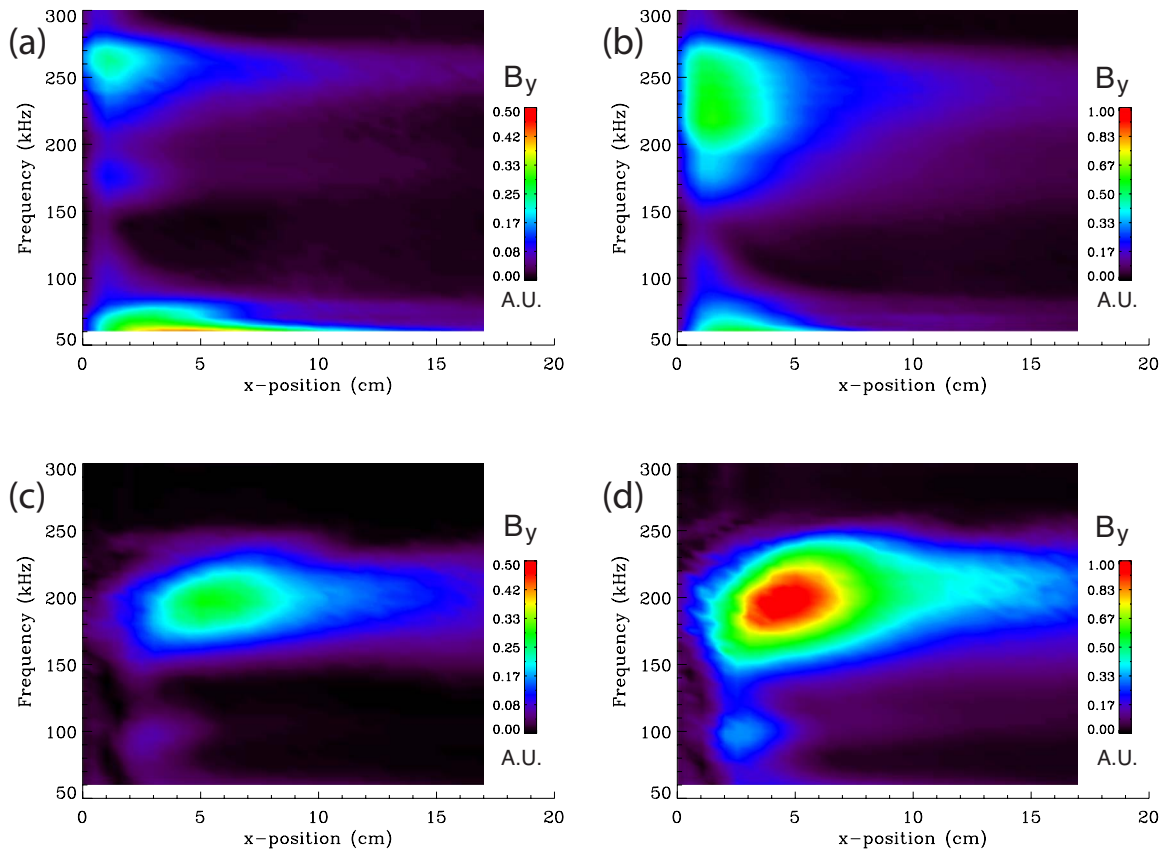
FIG. 11. (Color online) Contours of the amplitude of the y-component of the wave magnetic field as functions of launched frequency and position across the plasma column. Right panels correspond to an axial location 4.8 m from the antenna and left panels to 7.4 m. The top panels show measurements when the magnetic step sketched in Fig. 10 is present. Bottom panels correspond to a uniform magnetic field strength of 750 G, i.e., the same value as in the magnetic step case at the antenna location. The concentration ratio is 50/50 He/Ne.

other hand, waves above f_{ii}(1250 G) have relatively less decrease in amplitude, and there appears to be a propagation band between f_{ii}(1250 G) and f_{ci}(750 G). This propagation band does not have a sharp, lower frequency cutoff but it is similar in shape to the propagation bands shown in Fig. 9 for various concentration ratios. In contrast, no large decrease in amplitude is seen for the uniform magnetic field case, but rather a slight narrowing of the amplitude profile due to the radial spreading of the wave energy.

The behavior of the frequency profile measured at 4.8 m is further illuminated in Fig. 13. The frequency profiles for a uniform 750 G field and four "magnetic step" cases are shown. In the nonuniform cases, the strength of the high field is increased in steps of 100 G, ranging from 850 to 1150 G. As the step-up in field strength increases, the band of propagating frequencies moves toward higher frequencies and the wave amplitude decreases. This behavior is consistent with a decrease in radial spreading of the wave energy as the step-up in magnetic field value increases.

Figure 14 illustrates the axial evolution of the frequency profile for the case of a magnetic step from 750 to 1000 G. The technique consists of keeping the B-dot probe fixed in position (2 cm radial and 4.8 m axial) and changing the axial location of the ramp connecting the low and high-field regions of the step. The configuration is illustrated in the top panel of Fig. 14 and the measurements are shown in the bottom panel. In case (i) (solid/red line) the field is uniform

so that the step can be considered to take place far beyond the probe. In case (ii) (dashed/blue line) the increase in magnetic field strength begins at the probe location, and in case (iii) (dotted/black line) the probe is located some 2 m beyond the step, i.e., in the high-field region. The frequency profile is only slightly altered between case (i) and (ii), but the change in propagation band is clearly evident in case (iii). The profile in case (iii) still shows some wave amplitude at frequencies below f_{ii}(1000 G), but these waves are evanescent with a fairly long decay length so that their amplitudes would be lower further into the high-field region (as indicated in Fig. 12). Also the Bernstein feature evident in cases (i) and (ii) is greatly reduced in the high-field region [case (iii)], as the value of the neon gyrofrequency has increased.

V. CONCLUSIONS

This theoretical modeling study and experimental investigation have delineated the major properties of shear Alfvén waves of small transverse scale in a plasma with two ion species. The significance of transverse scales smaller than the ion-skin depth, c/ω_{pi}, is that intense parallel and transverse electric fields are generated. Large amplitude Alfvén waves in this parameter regime can cause significant electron acceleration and ion energization. Thus, the basic properties illustrated have consequences for a wide variety of studies including current and flow-drive scenarios in fusion devices,
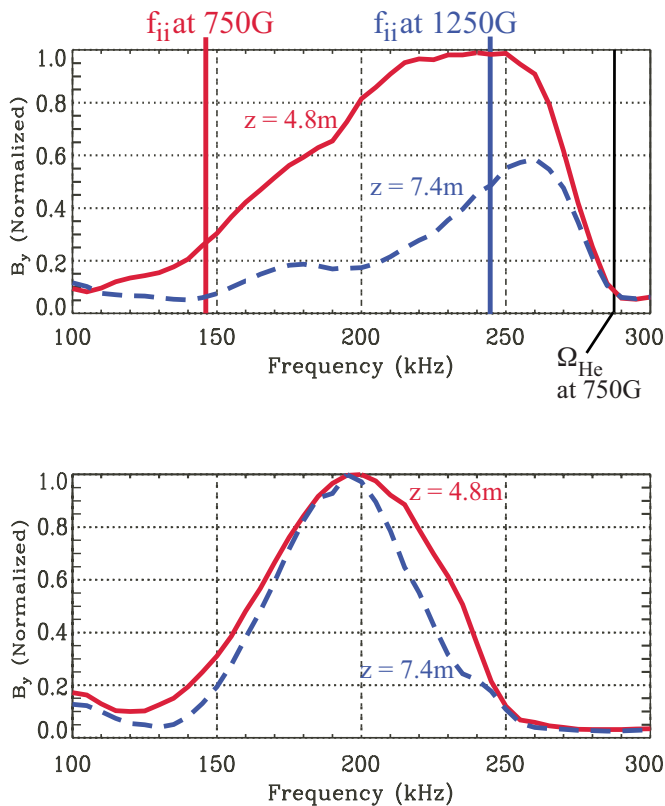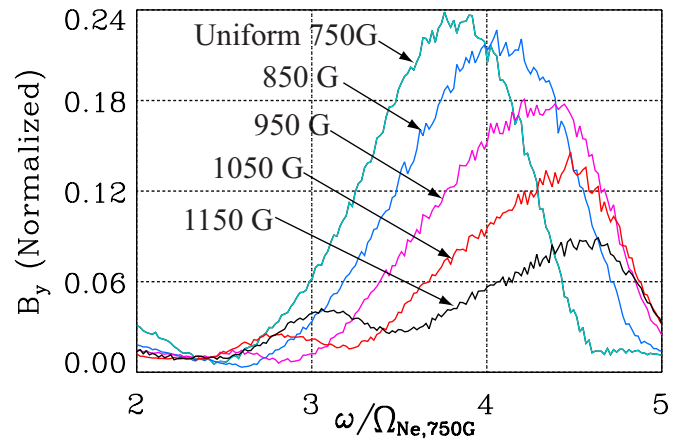
FIG. 13. (Color online) Frequency profile for different values of the field strength in the high-field side of the magnetic step. The strength is increased in steps of 100 G and the behavior for a uniform field at 750 G is included for reference. The magnetic field has the fixed value of 750 G at the antenna for all cases. Radial location is 2 cm and axial position 4.8 m. The concentration ratio is 50/50 He/Ne.

FIG. 12. (Color online) Top: amplitude of the y-component of the wave magnetic field in presence of magnetic step as a function of frequency, at a radial location of 2 cm for axial positions 4.8 and 7.4 m from the antenna. Waves below the ion-ion hybrid frequency in the high-field side are evanescent. Bottom: behavior for a uniform magnetic field strength of 750 G, i.e., the same value as in the magnetic step case at the antenna location. Signals in both panels are normalized to have the same value at 300 kHz. The concentration ratio is 50/50 He/Ne.

auroral ionosphere processes, modification of energetic ions in the earth's magnetosphere, and heating of the solar corona.

The key feature arising in the presence of two ion species is that the transverse component of the plasma dielectric tensor can vanish (i.e., $\varepsilon_\perp = 0$) for a wave frequency that lies between the cyclotron frequencies of each ion species. For ideal cold plasmas this causes a frequency propagation gap because the shear Alfvén waves become evanescent between the lowest cyclotron frequency and the ion-ion hybrid frequency. However, when finite ion temperature is considered the condition $\varepsilon_\perp = 0$ can be satisfied for multiple frequencies, traditionally associated with propagating, pure Bernstein modes. The studies reported here show that for finite ion temperature the shear waves can propagate between harmonics of the lowest cyclotron frequency, thus the single cold-plasma gap is replaced by multiple propagation bands. The prominence of these bands is theoretically predicted to increase with increasing ion temperature, as illustrated in Fig. 4. Wave propagation within these bands consists of a mixture of the cold-plasma cone trajectories and cross-field phase advance characteristic of Bernstein modes, as shown in Fig. 5. The conelike propagation features become dominant with increasing harmonic number, while at lower harmonic numbers the modes display a peak amplitude along field lines

connected to the source and display nearly perpendicular phase fronts.

Detailed measurements of the frequency dependence of shear waves launched in a helium-neon mix by an antenna of small transverse scale have confirmed the existence of propagation bands straddling the harmonics of the Ne cyclotron frequency, as illustrated in Fig. 8. The measured radial pattern of the radiated waves demonstrates that the higher frequencies exhibit the diverging cones typical of plasmas with a single ion species, while in the lowest harmonic band the pattern differs from the pure cone behavior.

Since, in the higher density plasmas used in this investigation, the techniques employed in previously published[33,34] studies to determine the species concentration ratio cannot be applied, a practical method described by Eq. (13) has been implemented. The method explicitly includes the important effect of the ionization potential of the atoms. From the observed frequency dependence of the radiated waves it is confirmed that Eq. (13) provides a useful gauge of the concentration ratio, although with a systematic error. It is also identified that since the cold-plasma gap is filled with finite ion temperature modes, a useful procedure to extract the value of the species concentration ratio from a direct measurement of the frequency dependence is to use the valley following the first peak as a marker for the ion-ion hybrid frequency, as illustrated in Fig. 9.

An increase in the strength of the confinement magnetic field (i.e., a magnetic step) greatly affects the propagation of shear Alfvén waves from the low-field to high-field regions in a two ion-species plasma. By examining the frequency dependence and the pattern of the measured signals for different values of the jump in magnetic field strength, it is concluded that wave reflection occurs when the condition $\varepsilon_\perp = 0$ is encountered along the ramp connecting the low-field region to the high-field region. This implies that the basic ingredient necessary for the creation of a two ion resonator in the presence of a nonuniform magnetic field has
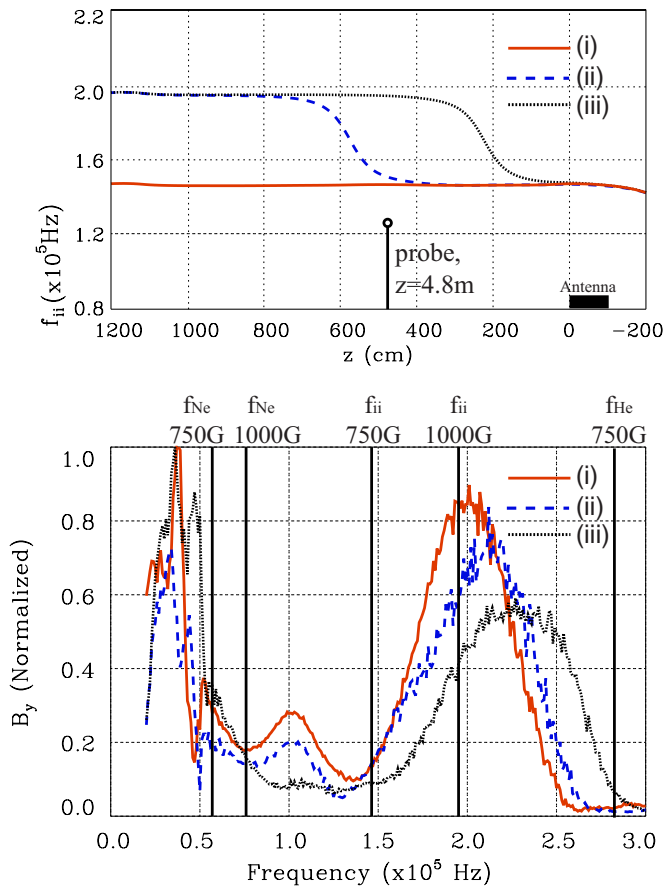
FIG. 14. (Color online) Top: three axial magnetic field profiles corresponding to the frequency dependencies shown in the bottom panel. Bottom: amplitude of the y-component of the wave magnetic field as a function of frequency, at a radial location of 2 cm for axial position 4.8 m. The concentration ratio is 50/50 He/Ne.

been demonstrated. This result warrants a future, focused investigation of a larger magnetic field configuration which allows the existence of two spatially separated reflection barriers. Such a study would provide a laboratory test of a proposed[30] natural resonator in planetary magnetospheres, and if free energy sources can be included, it would lead to a generalization of the single-species Alfvén wave maser.[42,43]

ACKNOWLEDGMENTS

[1] P. L. Auer, H. Hurwitz, and R. D. Miller, Phys. Fluids **1**, 501 (1958).
[2] T. H. Stix, *The Theory of Plasma Waves* (McGraw-Hill, New York, 1962), p. 18.
[3] A. G. Elfimov, R. M. O. Galvão, I. C. Nascimento, and G. Amarante-Segundo, Plasma Phys. Controlled Fusion **39**, 1551 (1997).
[4] B. Joye, A. Lietti, J. B. Lister, J.-M. Moret, and W. Simm, Phys. Rev. Lett. **56**, 2481 (1986).
[5] R. L. Lysak and Y. Song, J. Geophys. Res. **108**, 8005, doi:10.1029/2002JA009406 (2003).
[6] C. C. Chaston, C. W. Carlson, W. J. Peria, R. E. Ergun, and J. P. McFadden, Geophys. Res. Lett. **26**, 647, doi:10.1029/1998GL900246 (1999).
[7] K. G. McClements and L. Fletcher, Astrophys. J. **693**, 1494 (2009).
[8] S. Tomczyk, S. W. McIntosh, S. L. Keil, P. G. Judge, T. Schad, D. H. Seeley, and J. Edmondson, Science **317**, 1192 (2007).
[9] W. Gekelman, D. Leneman, J. Maggs, and S. Vincena, Phys. Plasmas **1**, 3775 (1994).
[10] W. Gekelman, S. Vincena, and D. Leneman, Plasma Phys. Controlled Fusion **39**, A101 (1997).
[11] C. Kletzing, S. Bounds, J. Martin-Hiner, W. Gekelman, and C. Mitchell, Phys. Rev. Lett. **90**, 035004 (2003).
[12] S. Vincena, W. Gekelman, and J. Maggs, Phys. Rev. Lett. **93**, 105003 (2004).
[13] D. J. Thuecks, C. A. Kletzing, F. Skiff, S. R. Bounds, and S. Vincena, Phys. Plasmas **16**, 052110 (2009).
[14] G. J. Morales, R. S. Loritsch, and J. E. Maggs, Phys. Plasmas **1**, 3765 (1994).
[15] G. J. Morales and J. E. Maggs, Phys. Plasmas **4**, 4118 (1997).
[16] F. S. Tsung, J. W. Tonge, and G. J. Morales, Phys. Plasmas **12**, 012508 (2005).
[17] G. Borg, M. H. Brennan, R. C. Cross, J. H. Lehane, and I. J. Donnelly, Plasma Phys. Controlled Fusion **27**, 1125 (1985).
[18] S. J. Buchsbaum, Phys. Fluids **3**, 418 (1960).
[19] R. L. Smith and N. Brice, J. Geophys. Res. **69**, 5029, doi:10.1029/JZ069i023p05029 (1964).
[20] P. Lee, R. J. Taylor, W. A. Peebles, H. Park, C. X. Yu, Y. Xu, N. C. Luhmann, Jr., and S. X. Jin, Phys. Rev. Lett. **49**, 205 (1982).
[21] A. K. Ram, A. Bers, S. D. Schultz, and V. Fuchs, Phys. Plasmas **3**, 1976 (1996).
[22] H. Ikezi, J. S. Degrassie, R. I. Pinsker, and R. T. Snider, Rev. Sci. Instrum. **68**, 478 (1997).
[23] G. W. Watson, W. W. Heidbrink, K. H. Burrell, and G. J. Kramer, Plasma Phys. Controlled Fusion **46**, 471 (2004).
[24] A. K. Singh, A. K. Singh, D. K. Singh, and R. P. Singh, J. Atmos. Sol.-Terr. Phys. **60**, 551 (1998).
[25] Y. Lin, S. Wukitch, P. Bonoli, E. Nelson-Melby, M. Porkolab, J. C. Wright, N. Basse, A. E. Hubbard, J. Irby, L. Lin, E. S. Marmar, A. Mazurenko, D. Mossessian, A. Parisot, J. Rice, and S. Wolfe, Phys. Plasmas **11**, 2466 (2004).
[26] M. Temerin and R. L. Lysak, J. Geophys. Res. **89**, 2849, doi:10.1029/JA089iA05p02849 (1984).
[27] T. Intrator, M. Vukovic, A. Elfimov, P. H. Probert, and G. Winz, Phys. Plasmas **3**, 1054 (1996).
[28] F. W. Perkins, Nucl. Fusion **17**, 1197 (1977).
[29] Y. Lin, J. E. Rice, S. J. Wukitch, M. J. Greenwald, A. E. Hubbard, A. Ince-Cushman, L. Lin, E. S. Marmar, M. Porkolab, M. L. Reinke, N. Tsujii, J. C. Wright, and Alcator C-Mod Team, Phys. Plasmas **16**, 056102 (2009).
[30] A. V. Gigliemi, A. S. Potapov, and C. T. Russell, Pis'ma Zh. Eksp. Teor. Fiz. **72**, 432 (2000); JETP Lett. **72**, 298 (2000).
[31] G. G. Borg and R. C. Cross, Plasma Phys. Controlled Fusion **29**, 681 (1987).
[32] J. P. M. Schmitt, Phys. Rev. Lett. **31**, 982 (1973).
[33] H. Kojima, H. Sugai, and T. Okuda, Plasma Phys. Controlled Fusion **26**, 359 (1984).
[34] M. Ono, Phys. Rev. Lett. **42**, 1267 (1979).
[35] D. M. Suszcynsky, R. L. Merlino, and N. D'Angelo, IEEE Trans. Plasma Sci. **16**, 396 (1988).
[36] G. G. Borg, J. Plasma Phys. **59**, 151 (1998).
[37] B. D. Fried, C. L. Hedrick, and J. McCune, Phys. Fluids **11**, 249 (1968).
[38] W. Gekelman, H. Pfister, Z. Lucky, J. Bamber, D. Leneman, and J. E. Maggs, Rev. Sci. Instrum. **62**, 2875 (1991).
[39] M. Ono, M. Porkolab, and R. P. H. Chang, Phys. Fluids **23**, 1656 (1980).
[40] C. C. Mitchell, J. E. Maggs, S. T. Vincena, and W. N. Gekelman, J. Geophys. Res. **107**, 1469, doi:10.1029/2002JA009277 (2002).
[41] Y. Zhang, W. W. Heidbrink, H. Boehmer, R. McWilliams, G. Chen, B. N. Breizman, S. Vincena, T. Carter, D. Leneman, W. Gekelman, P. Pribyl, and B. Brugman, Phys. Plasmas **15**, 012103 (2008).
[42] J. E. Maggs, G. J. Morales, and T. A. Carter, Phys. Plasmas **12**, 013103 (2005).
[43] G. J. Morales and J. E. Maggs, Phys. Plasmas **13**, 052109 (2006).